Journal of Catalysis **182,** 400–416 (1999)
Article ID jcat.1998.2337, available online at http://www.idealibrary.com on IDEAL®

Effect of Zeolite Structure and Acidity on the Product Selectivity and Reaction Mechanism for *n*-Octane Hydroisomerization and Hydrocracking

Wenmin Zhang and Panagiotis G. Smirniotis[1]

Department of Chemical Engineering, University of Cincinnati, Cincinnati, Ohio 45221–0171

Received June 17, 1998; revised November 18, 1998; accepted November 19, 1998

The activity, product selectivity, and stability of a series of bifunctional zeolite catalysts, primary ZSM-12, USY, and β-zeolite, with different Si/Al ratios were compared for the hydroisomerization and hydrocracking of *n*-octane. The performance of L-zeolite and mordenite was examined to a lesser extent as well. It was found that the activity per acidic site decreases at the initial stage (1 h on stream) in the following order: ZSM-12 > β-zeolite > mordenite > USY > L-zeolite. For extended periods of operation, the activity of ZSM-12 remains unchanged. The superior stability of ZSM-12 even under accelerating coking conditions results from its unique pore structure, which does not favor coke formation. Its one-dimensional noninterpenetrating puckered channels (5.5 × 6.1 Å) act as perfect tubes, which do not trap coke precursors. The branched product selectivity increases with the increase in Brønsted acid site strength of the zeolite catalysts, and thus hydroisomerization is favored at the expense of cracking at a higher Brønsted acid strength. USY-5.8 (CBV-712) showed relatively high initial activity with respect to other USYs. This is probably related to its high surface Al content. The Brønsted acid strength of the USY zeolites decreases in the order USY-2.6 > USY-28 ≥ USY-5.8. The 2,2-DMC_6 and 3,3-DMC_6 isomers are not favored as final products due to their bulky molecular size even in USY. In addition, the 2,2-DMC_6 species is more abundant than 3,3-DMC_6 because the rate of isomerization by PCP intermediates decreases in the following order: 2-MC_7 > 3-MC_7 > 4-MC_7. The 2,3-DMC_6 concentration is much higher than that predicted by equilibrium, which indicates that the interconversion of 2,3-DMC_6 to other dibranched isomers is not preferred. The i-C_4/*n*-C_4 ratio detected depends on both the reaction temperature and zeolite pore structure/acidity. Aluminium content determines the type of β-scission. For zeolites with a high concentration of acid sites (Si/Al < about 30), type A β-scission dominates at low temperature, while at lower Al content, type A, B, and C β-scissions are equally important.

Key Words: **ZSM-12; USY; β-zeolite; *n*-octane; hydroisomerization; hydrocracking; time-stable catalysts.**

INTRODUCTION

The hydroisomerization of *n*-paraffins is of considerable interest and plays an important role in the petroleum industry, because it provides branched paraffins which inherently possess higher octane numbers than *n*-paraffins. Bifunctional catalysts with an acidic function balanced by the metal function have shown high efficiency in hydroisomerization of *n*-paraffins (1, 2). It is well established that over zeolites the isomerization of *n*-paraffins proceeds through consecutive branching reactions while cracking reactions occur in parallel with the isomerization; and multibranched paraffins are more susceptible to cracking than monobranched ones (2, 3). However, it is still not clear how the strength of the zeolite acidic site affects the reaction mechanism and the product selectivities, especially those of the branched products.

The aim of this work is to investigate the effect of the strength of acid sites and the pore structure of selected 12-membered-ring (MR) large-pore zeolites, namely, ZSM-12, β-zeolite, USY, mordenite (8-MR pores exist as well), and L-zeolite on the product selectivities, reaction mechanisms, and time-on-stream stability.

EXPERIMENTAL

Catalyst Preparation

In this study, parent ZSM-12 (Si/Al = 35) and β-zeolite (Si/Al = 15) were hydrothermally synthesized from the corresponding aluminosilicate gels. Details about the preparation procedures can be found in our previous work (4). The synthesized parent zeolites were calcined in air at 520°C for 4 h to burn the occluded template, and then were dealuminated with hydrochloric acid. Different levels of dealumination were achieved by varying the concentrations of HCl solutions in the range 1 to 7 N HCl in a 1-liter flask. Two grams of zeolites was used in each batch of dealumination. It should be noted that ZSM-12 does not lose its crystallinity even at the highest dealumination severity.

[1] To whom all correspondence should be addressed. E-mail: Panagiotis.Smirniotis@Uc.Edu.

0021-9517/99 $30.00

The USY samples were obtained from PQ Corporation. Controlled steam treatment followed by lean acid leaching of the parent zeolite USY (CBV-100) was involved in the synthesis of the dealuminated USY-5.8 (CBV-712) sample. The CBV-712 sample was subject to severe acid leaching for the synthesis of the USY-28 (CBV-760) sample. Mordenite and L-zeolites were kindly donated to us from UOP. Ammonium hexafluorosilicate was employed for the dealumination of mordenite and L-zeolite. An appropriate amount of $(NH_4)_2SiF_6$ dissolved in 200 ml H_2O was added dropwise within 2 h, and kept at 90°C with stirring for 24 h. The ammonium form of the zeolites was obtained by cation exchange of the dealuminated zeolites with a 2.0 N NH_4Cl solution at 90°C for 4 h. Finally, the zeolites were transformed to their protonated form by calcination in air at 450°C for 1 h. The loading of Pt on the catalysts (0.5 wt%) was conducted with wet impregnation of H_2PtCl_6 solution (Aldrich, 8 wt% solution in water). The catalysts were dried overnight in an oven at 120°C. The physical properties of the zeolites are listed in Table 1. Each zeolite is designated as its name followed by its bulk Si/Al ratio.

X-ray diffraction was employed for identification of the synthesized zeolites and for determination of the crystallinity of the dealuminated zeolites. The estimation of the crystallinity was based on the areas under the main crystallographic peaks of each zeolite. The bulk Si/Al ratios were measured by wet analysis involving ICP spectroscopy. For the analysis, lithium metaborate was used for the fusion of zeolite powders (900°C), which subsequently were dissolved in HNO_3 solution. The sodium content was extremely low for the majority of the protonated zeolites.

TABLE 1

Zeolite Physical Properties

Zeolite	Dealumination agent/ method	Si/Al (bulk)	Crystallinity
ZSM-12-35	As synthesized	35	100
ZSM-12-40	1.0 N HCl	40	≈100
ZSM-12-54	3.0 N HCl	54	≈100
ZSM-12-58	4.0 N HCl	58	≈100
ZSM-12-69	5.0 N HCl	69	≈100
Beta-15	As synthesized	15	100
Beta-85	5.0 N HCl	85	79
Beta-132	7.0 N HCl	132	90
USY-2.6(CBV-100)[a]		2.6	100
USY-5.8(CBV-712)[a]	Steaming + lean acid leaching	5.8	81
USY-28(CBV-760)[a]	Steaming + strong acid leaching	28.0	72
MOR-9.5[b]		9.5	100
MOR-36	25 g $(NH_4)_2SiF_6$	35.7	71
LTL-3.8[b]		3.8	100

[a] Provided by PQ Corporation.
[b] Provided by UOP.

Acidity Measurement

The quantitative characterization of the zeolite surface acidity (Brønsted and Lewis acid sites) was carried out with NH_3-stepwise temperature-programmed desorption (NH_3-STPD) experiments. The desorption curve consists of five distinct peaks occurring at the following optimized temperature ranges: 150 to 180°C, 180 to 250°C, 250 to 350°C, 350 to 440°C, 440 to 540°C. By coupling this technique with NH_3 FT-IR, it was found that the first two peaks are mainly weak and stronger Lewis acid sites, as well as weak Brønsted sites. The other three peaks are Brønsted acid sites (IR stretching frequency of NH_4^+ on AlO^-) of increasing strength (5, 6). The desorption started at 150°C to exclude any physisorbed ammonia.

The sample of each protonated zeolite (50 mg) was held by small plugs of Pyrex glass wool located in the middle of a 6-mm-i.d. tube. Before starting the ammonia adsorption, each sample was cleaned by purging He at 550°C for 1 h. Then, anhydrous ammonia (4% in He) was admitted to the sample for 1 h at 150°C to ensure the saturation of all acidic sites of the zeolite. Helium was thereafter sent to the bed to purge any physically adsorbed ammonia. This step was maintained until no NH_3 desorption was observed. Then, the NH_3-STPD profile, which consisted of isothermal steps followed by steps of increasing temperature with a constant rate, was started. The desorption experiment followed a profile that started at 150°C and reached the targeted temperatures (180, 250, 350, 440, and 540°C). After reaching each temperature the bed temperature was held constant for 60 min and then it was raised to the next temperature within 30 min. Blank experiments confirmed that at any desorption temperature the background was stable. The STPD experiments were repeated several times and good reproducibility was obtained.

Catalytic Experiments

n-Octane (Aldrich, >99.5% purity) was used as the probe molecule. The impurities were mainly 3-methylheptane and 2,2,4-trimethylpentane, and they were excluded in calculating the product selectivities. The experiments were carried out in a flow reactor system incorporating a $\frac{1}{4}$-in.-o.d. stainless-steel reactor. The catalysts were activated *in situ* by oxidation with high-purity oxygen for 1 h at 450°C, followed by purging with ultrahigh-purity He (Wright Brothers, 99.998%) for 15 min. The reduction of the catalyst was carried out at 450°C in high-purity H_2 for 1 h at atmospheric pressure. For the catalytic experiments, H_2 was provided from the gas cylinder to the reactor while the pressure regulation was achieved with a backpressure regulator placed at the exit of the reactor tube. In all the experiments, 50 mg of fresh catalyst was loaded on top of a glass wool plug. The feed was introduced into the reactor at a predetermined flow rate through a special septum injection port into the

heated line using a liquid infusion pump (Cole–Parmer) or a syringe pump (ISCO Model 100DM) in the case of time-on-stream experiments.

The product identification was accomplished by a high-resolution gas chromatograph (Hewlett–Packard, 5890 Series II) equipped with a mass spectrometer (Hewlett–Packard, 5972 Series II). The reactor effluent stream was sent for analysis through a heated line (about 180°C) to the gas chromatograph. The GC/MS unit was attached to a PC unit for data acquisition and processing. The GC was equipped with a high-performance capillary column (SUPELCO Petrocol DH50.2, fused silica with bonded dimethylsiloxane, 0.2-mm i.d., 50-m length, and 0.5-μm film thickness). By optimizing the flow of carrier gas in the column and the temperature profile in the GC oven, we achieved efficient separation of all the products of the reaction.

The reaction was carried out under a wide range of operating conditions: temperature, 180–450°C; liquid feed flow rate, 0.03–8.0 cm^3/h; H_2 flow rate, 4–320 cm^3/min; total pressure, 100 psig. With the exception of the time-on-stream experiments, all the data were collected at 1 h on stream.

The product selectivities (mol or wt%) are defined as the concentration of the individual component over the concentration of all products in the effluent stream.

RESULTS AND DISCUSSION

Zeolite Surface Acidity

NH_3-STPD coupled with FT-IR enables us not only to distinguish Brønsted and Lewis acidic sites, but also to quantify the number of acid sites with different strength. As proved in our previous work (5, 6), we can obtain up to five distinct desorption peaks of NH_3 chemisorbed on acid sites in the range 150 to 540°C. According to FT-IR experiments carried out at the same NH_3 desorption temperature, the first two peaks in the NH_3-STPD response are believed to be Lewis acid sites, and weak Brønsted sites. With the exception of USY the other three peaks are Brønsted acid sites. For the USY samples, due to the incomplete separation of Lewis and Brønsted sites for the first three peaks in STPD, the deconvolution of STPD peaks based on the IR spectra was used to obtain the numbers of Brønsted and Lewis acid sites. The acidity characteristics of the different zeolites used are presented in Tables 2 and 3. To quantitatively evaluate the average strength of the strong sites (last three peaks in STPD experiments), we introduce, T_B, the average desorption temperature of NH_3 from strong acid sites, which is defined as

$$T_B = \frac{350\,(\text{area of third peak}) + 440\,(\text{area of fourth peak}) + 540\,(\text{area of fifth peak})}{\text{total area of third, fourth, and fifth peaks}}.$$

For ZSM-12, at any extent of dealumination, about 50% of the total number of acid sites correspond to weak Brønsted sites (peak 3 in Table 2). Moreover, the dealumination results in an increase in the ratio of the total number of strong sites with respect to weak sites (Table 3). For any extent of dealumination used in this study, the above ratio reaches a value of about 3. The average NH_3 desorption temperature from strong acid sites, T_B, decreases with dealumination over ZSM-12, which indicates a slight decrease in the average acid site strength. In contrast, for β-zeolite, with an increase in the Si/Al ratio, the percentage of medium and strong Brønsted sites increases, and T_B

TABLE 2

Area Percentage of Different Ammonia Desorption Peaks That Correspond to Lewis and Brønsted Acid Sites of Variable Strength Determined by NH_3-STPD Experiments

Zeolite	Area (%)						T_B (°C)[a]
	Si/Al (bulk)	Peak 1	Peak 2	Peak 3	Peak 4	Peak 5	
ZSM-12-35	35	11.3	21.0	42.0	13.3	12.4	404.4
ZSM-12-40	40	7.5	16.4	48.9	10.7	16.6	405.4
ZSM-12-54	54	6.7	18.8	48.8	8.7	16.7	403.5
ZSM-12-58	58	6.1	19.6	54.3	8.0	12.1	391.7
ZSM-12-69	69	6.6	19.3	51.7	9.5	12.9	395.9
Beta-15	15	10.3	22.2	27.8	19.2	20.5	436.1
Beta-85	85	7.0	23.3	27.8	19.1	22.7	439.4
Beta-132	132	8.4	25.6	22.0	20.6	23.5	448.7
USY-2.6	2.6	12.6	33.1	28.7	12.2	13.5	419.6
USY-5.8	5.8	13.5	35.5	36.4	7.5	7.1	391.1
USY-28	28.0	9.4	35.6	33.1	10.3	11.7	409.0
MOR-9.5	9.5	7.0	9.5	23.1	34.6	25.9	446.1
MOR-36	35.7	5.5	9.0	41.7	30.9	12.9	414.8
LTL-3.8	3.8	10.0	33.3	37.1	9.8	9.9	400.4

[a] Average NH_3 desorption temperature from strong acid sites (last three peaks).

TABLE 3

Acidity Characteristics of the Zeolites as Determined by NH_3-STPD

Zeolite	Si/Al (bulk)	ml NH_3 (STP)/g	No. NH_3/ No. Al	Strong/ weak
ZSM-12-35	35	10.4	0.98	2.09
ZSM-12-40	40	8.8	0.96	3.19
ZSM-12-54	54	6.8	0.99	2.91
ZSM-12-58	58	6.9	1.09	2.89
ZSM-12-69	69	5.7	1.06	2.87
Beta-15	15	24.6	1.01	2.08
Beta-85	85	4.0	0.91	2.30
Beta-132	132	2.7	0.94	1.94
USY-2.6	2.6	25.6	0.24	1.19
USY-5.8	5.8	12.0	0.47	1.04
USY-28	28.0	5.2	0.87	1.22
MOR-9.5	9.5	29.3	0.81	5.08
MOR-36	35.7	9.3	0.91	5.90
LTL-3.8	3.8	28.2	0.27	1.31

increases. Thus, the average Brønsted acid site strength increases with dealumination. On the other hand, the number of total acid sites decreases significantly with the increase in the Si/Al ratio as expected. Other researchers using CO as probe base found a similar trend, namely, an increase in strength of Brønsted sites with the dealumination of β-zeolite (7). Regardless of the dealumination level, the ratio of strong to weak acid sites of β-zeolite remained in the vicinity of 2. It is worthwhile to note that for both ZSM-12 and β-zeolites there is a one-to-one relation (Table 3) between the NH_3 molecules chemisorbed on all acid sites and the total number of Al atoms (nonframework and framework), which indicates that ammonia effectively probes all the acid sites.

One, however, can see that the parent USY (USY-2.6) has the highest percentage of medium and strong Brønsted sites (peak 4 and 5 in Table 2) among all the USYs tested. The increase in the severity of steam treatment decreases the relative population of medium and strong Brønsted acid sites (compare the USY-2.6 and USY-5.8 samples in Table 2). Other researchers also observed that by increasing steam severity, the strength of Brønsted acid sites and the ratio of Brønsted/Lewis sites decrease (8). It is interesting to note that after severe acid leaching of the steam dealuminated USY sample (USY-5.8) to generate USY-28, the Brønsted acid site strength of the sample increases again (Table 2). Thus, one may conclude that when steam treatment is involved in dealumination, Brønsted sites are preferentially removed, while when acid leaching is used, Lewis acid sites and weak Brønsted sites are extracted first. The decrease in the average strong acid site strength index, T_B, in the sequence USY-2.6 > USY-28 $\geq$ USY-5.8, is consistent with the above discussion.

It seems that the ratio of strong to weak acid sites (B/L) is a characteristic property of different zeolites, and it does not change very much with the Si/Al ratio. As shown in Table 3, very different values of the B/L ratio were observed for each zeolite, i.e., about 2 for β-zeolite, about 1.5 for USY, about 3 for dealuminated ZSM-12, and about 5 for mordenite. Moreover, the amount of NH_3 adsorbed per Al atom can be lower than one. We observed that for zeolites with inherently high aluminum content such as USY, mordenite, and L-zeolite, when the Si/Al ratio is below about 20, the number of ammonia molecules chemisorbed per number of Al atoms (bulk) is lower than unity. This trend was observed over the above three zeolites reproducibly and indicates that probably at high concentrations of Al, each ammonia molecule is associated with more than one acid site and/or all the aluminum sites are not equally accessible to ammonia molecules.

Catalyst Activity

The effect of the Si/Al ratio of different zeolites on the catalytic activity is shown in Fig. 1. Different conversions were obtained by varying the reaction temperatures in the range 195 to 415°C. The catalytic activity of ZSM-12 decreases with the increase in Si/Al ratio. This is as expected since by increasing the Si/Al ratio the Al content of the zeolites decreases; that is, the number of acid sites decreases. β-Zeolite demonstrates behavior similar (Fig. 1b) to that of ZSM-12.

In contrast, this monotonic decrease in activity was not observed over the dealuminated USY zeolites (Fig. 1c). USY-5.8 demonstrates a higher activity than its parent zeolite USY-2.6 at any temperature, although it possesses less Al. Haag and Lago (9) observed a similar behavior, namely, steam dealuminated Y faujasite is more active than its parent zeolite for catalytic cracking reactions. The same trend in activity was also observed over steam dealuminated ZSM-5 for *n*-heptane cracking (10) and steam dealuminated mordenite for the disproportionation reaction of *o*-xylene (11). The latter group attributed this increase in disproportionation reactions to the formation of Lewis acid sites during the steam dealumination.

In fact, as one can see from our STPD results in Table 2, USY-5.8 has the lowest average strong acid site strength among the three USY zeolites used. Thus, the enhancement of activity cannot be attributed to the increased number or strength of strong sites since both of them decrease with steam dealumination. A similar conclusion was obtained recently by other researchers (12, 13).

Our XPS investigations indicate that the USY-5.8 sample possesses uneven Al distribution in comparison with the other samples tested. Significantly higher Al concentrations were detected on the surface of the USY-5.8 than on other USY samples. We believe that the increased activity of USY-5.8 is due to this high surface Al content generated by the steam treatment. The treatment with steam removed Al from framework tetrahedral positions, which migrated to the surface. Others (14) also found that steam dealuminated USY samples (CBV families) have a much higher content of surface Al than the as-synthesized parent USY. They also found that steam-only dealuminated Pt/HUSY catalysts were more active than either parent or further acid-leached USYs for the hydroisomerization of *n*-heptane and *n*-decane. This indicates that the intracrystalline mass transfer resistance at this range of temperature plays some role even with large-pore zeolites like USY (15). It is also reported that the HY-zeolite crystallites are severely diffusion limited for the cracking of long-chain paraffins; and the reduction of crystallite size increases the cracking activity of HY and reduces isomerization (16, 17). Dadyburjor and Bellare (18) also found that there exists a strong diffusion resistance for the cumene cracking reaction over REY zeolites in the temperature range 225–575°C. It is worth noting that further dealumination by acid leaching (from CBV-712 to CBV-760) establishes uniformity of the aluminum distribution in the zeolite crystals (14). Indeed, our catalytic results (Fig. 1c) validate the above changes in

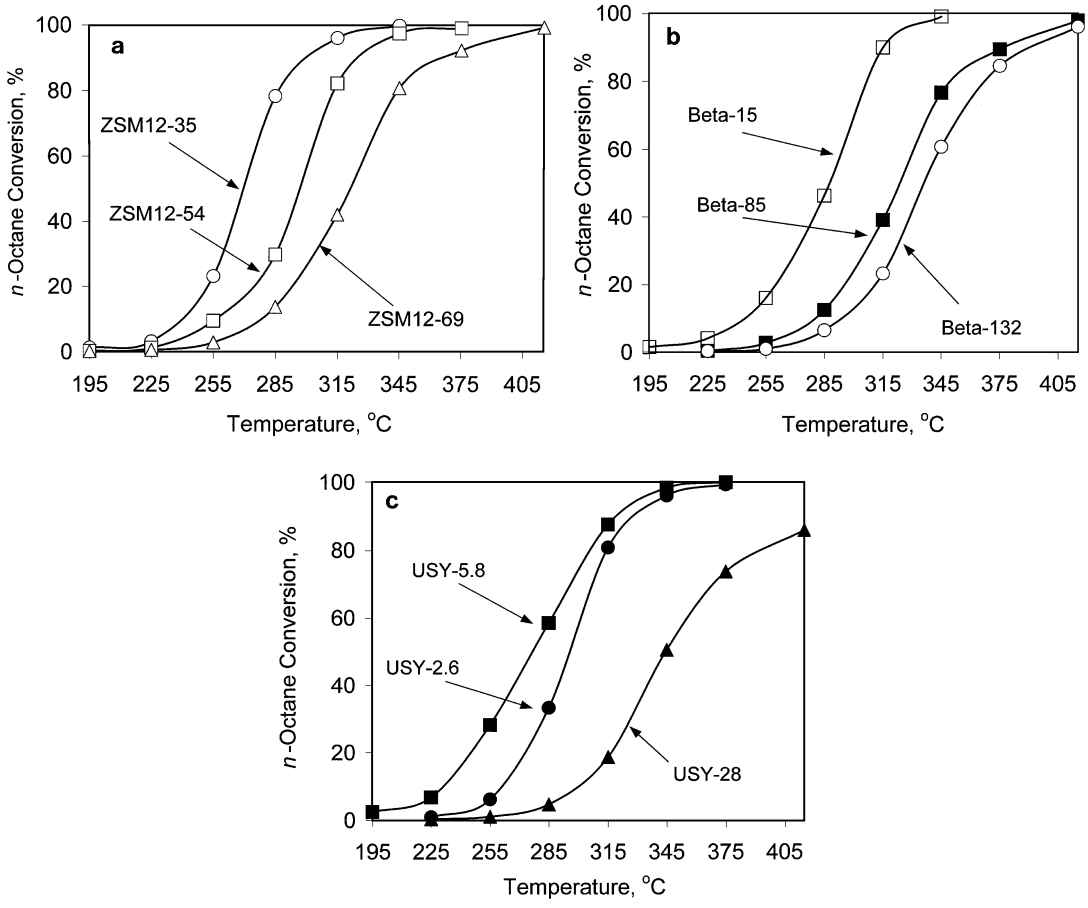

FIG. 1. *n*-Octane conversion versus temperature over (a) Pt/HZSM-12, (b) Pt/HBeta, and (c) Pt/HUSY at WHSV = 7 h^{-1}, $H_2/n\text{-}C_8$ (mole) = 16, total pressure of 100 psi, and Pt loading level of 0.5 wt%.

the Al distribution of USY as a function of the method and extent of dealumination. USY-5.8 is the most active catalyst among all the USYs used at any reaction temperature, followed in activity by USY-2.6 (even though the latter one is richer in Al). USY-28 acquires the lowest activity as expected. USY-28 is also the least active at any temperature in comparison even with the most severely dealuminated ZSM-12 and β-zeolite, though they possesses much higher Si/Al ratios (69 and 132, respectively).

A comparison between different types of zeolite catalysts based on turnover frequencies at 285°C (after 1 h on stream, Table 4) reveals that ZSM-12 is generally more active than all other zeolites. One reason for this behavior is that the ZSM-12 samples have relatively high strong/weak acid site ratios as shown in Table 3. If the strong sites are considered as being the active sites for the reaction, the difference in TOF values becomes smaller. This would agree with the general belief that only Brønsted acid sites are strong enough to catalyze the skeletal isomerization and cracking reactions of alkanes at current mild reaction temperatures. Additional supportive evidence indicates (19) that Lewis acid sites (acid sites corresponding to NH_3-TPD desorption temperature <250°C) play no role in the *n*-hexane isomerization at the reaction temperature of 200°C. From our work we observed that at comparable Si/Al ratios and 1 h on stream, the zeolite activity decreases in the following order:

$$\text{ZSM-12} > \beta\text{-zeolite} > \text{mordenite} > \text{USY} > \text{L-zeolite}.$$

It is worth noting that ZSM-12 with Si/Al = 35 is much more active than USYs although the latter ones contain significantly higher number of Al atoms. The activity of ZSM-12, however, decreases rapidly with dealumination. The TOF of ZSM12-69 is lower than that of Beta-85 (Table 4).

Product Distribution versus Zeolite Pore Structure

The product distribution over the zeolite catalysts investigated at comparable *n*-octane conversion in the vicinity of about 50% is shown in Table 5. The same types of products are obtained over all catalysts, which include in general (a) isooctanes (monobranched and dibranched C_8 paraffins, and trace amounts of trimethylpentanes), (b) cracked products (light hydrocarbons) with carbon number less than

TABLE 4

Turnover Frequency (s^{-1}) of Different Zeolite Catalysts for the *n*-Octane Conversion at 285°C Based on Different Definitions[a]

Zeolite	Based on all acid sites[b] ($\times 10^{-3}$)	Based on strong sites[c] ($\times 10^{-3}$)	Based on all Al atoms[d] ($\times 10^{-3}$)
ZSM-12-35	28.3	39.4	27.7
ZSM-12-54	12.8	16.7	12.7
ZSM-12-69	8.9	12.2	9.4
Beta-15	8.6	12.7	8.7
Beta-85	11.7	16.7	10.6
Beta-132	9.4	14.4	8.8
USY-2.6	5.0	13.3	1.1
USY-5.8	18.9	37.2	8.9
USY-28	3.3	6.1	2.9
MOR-9.5	8.7	10.2	7.0
MOR-36	5.5	6.4	5.0
LTL-3.8	2.7	4.8	0.7

[a] Catalyst weight, 50 mg; *n*-octane feed rate, 0.5 cm^3/h; H_2/*n*-C_8, 16; total pressure, 100 psig; 1 h on stream.

[b] Based on the NH_3-STPD experiments (all desorption peaks were included).

[c] Based on the acid sites with NH_3 desorption from last three peaks.

[d] Based on Al amount from elemental analysis (ICP spectroscopy).

8, and (c) trace amounts of toluene, xylene, and C_5 and C_6 naphthenes at relatively high temperatures. Products with more than eight carbon numbers were not observed. Methane was not detected under a wide range of the operating conditions involved, thus excluding the existence of hydrogenolysis reactions of the feed occurring over metal sites.

As expected, USY and β-zeolites, due to their relatively large pore sizes, allow to a higher extent the branching of C_8 paraffins at the same level of *n*-octane conversion in comparison with ZSM-12 (Table 5). Trace amounts of tribranched C_8 as final products are observed over USY and β-zeolite catalysts. USY has a tridimensional channel structure with an aperture size of 7.4 Å, and β-zeolite consists of 12-membered-ring pores of linear channels of about 7.3×6.5 Å and tortuous channels of 5.5×5.5 Å. Its channel intersections of about 10 Å and render the structure tridimensional (20). ZSM-12 possesses one-dimensional noninterconnecting tubular-like channels (5.5×6.1 Å) (21). Tribranched C_8 paraffins with a critical molecular diameter of about 7.0 Å (22) were not detected as final products over ZSM-12 at the current reaction temperatures used. This is partially because of the relatively high temperatures, which do not favor thermodynamically the formation of tribranched isomers. Moreover, the fast cracking of the latter hydrocarbons is responsible for the absence of tribranched hydrocarbons in the final products. Dibranched alkane molecules, even those with two branches on the same carbon of the main chain, such as 2,2-dimethylhexane (2,2-DMC_6), 3,3-dimethylhexane (3,3-DMC_6), and even 3-ethyl-2-methylpentane (3-E, 2-MC_5), were observed in the products. This is not as expected because their sizes are comparable to those of tribranched isomers as suggested in the references (22, 23). Indeed, we found (24) that 2,2,4-trimethylpentane in this temperature range can diffuse even in the pores of ZSM-12 and further cracked to lighter hydrocarbons. This means that the effective pore size of ZSM-12 is larger than its crystallographic pore diameter. Other researchers (25) suggested that the openings of ZSM-12 are larger (5.6×7.7 Å) than what is commonly believed. Similarly, it was also reported (26) that the effective pore dimensions of mordenite were 8.2–8.6 Å, which is 1.5–1.6 Å larger than the calculated crystallographic values.

It is well established that the hydroisomerization reactions proceed through successive mono-, di-, and tribranched intermediates formed by type A (methyl shift) and B [via protonated cyclopropane (PCP)] isomerization mechanisms. The former type of isomerizations results in products with the same number of branches as the reactant. Isomerizations via PCP intermediates are responsible for the net increase or decrease in the extent of branching of the reaction products. At the same time, hydrocracking follows type A (tertiary carbenium ion to tertiary), B1 (secondary carbenium ion to tertiary), B2 (tertiary to secondary), C (secondary carbenium ion to secondary), and D (secondary carbenium ion to primary) β-scissions (1, 16, 27, 28). Our experiments agree with the above reaction mechanisms even for zeolites with high Si/Al ratios, which were not commonly discussed in the past. As shown in Fig. 2, at a very short space time, isomers are the only primary products over USY-28. The selectivity of isomers passes through a maximum, which is a typical behavior of consecutive reactions. The rate of hydrocracking, as a secondary reaction, increases rapidly with the space time. Other zeolites followed a similar behavior.

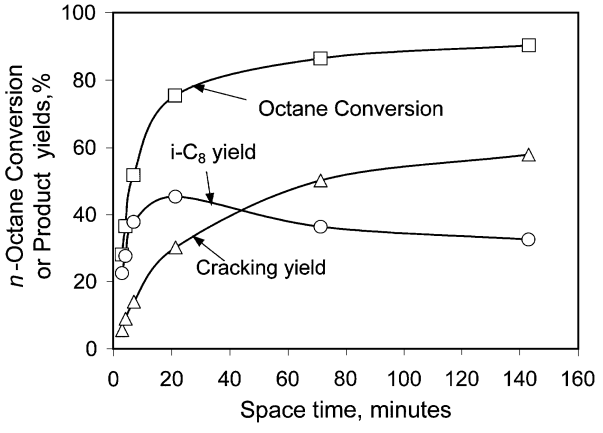

FIG. 2. *n*-Octane conversion versus space time over Pt/HUSY-28 at 330°C, H_2/*n*-C_8 (mole) = 16, total pressure of 100 psi, and Pt loading level of 0.5 wt%.

TABLE 5

Product Selectivities (mol%) of *n*-Octane over Different Zeolite Catalysts[a]

Product[b]	ZSM-12-35	ZSM-12-69	Beta-15	Beta-132	USY-2.6	USY-28	MOR-9.5	MOR-36	LTL-3.8
C_1									
C_2	0.2	0.1					0.3		
C_3	15.8	21.7	17.1	11.5	7.1	3.5	24.6	16.9	14.5
i-C_4	15.5	16.8	32.4	12.4	8.3	8.2	35.0	24.2	20.4
n-C_4	11.5	14.8	18.5	8.6	4.7	3.4	14.8	11.8	11.7
i-C_5	9.1	11.2	11.6	6.8	4.6	2.8	13.4	9.5	9.6
n-C_5	4.8	8.0	3.1	3.0	0.5	0.4	2.9	2.0	1.6
DMC_4			0.02				0.05		
2-MC_5	0.03	0.02	0.07				0.4	0.06	0.1
3-MC_5	0.02	0.01	0.04		0.01		0.2	0.04	0.2
n-C_6	0.05	0.06	0.05		0.02	0.04	0.2	0.06	0.1
DMC_5									
2-MC_6	0.02		0.03				0.10		0.04
3-MC_6	0.01	0.00	0.02				0.09		0.03
n-C_7	0.05	0.03	0.04		0.07	0.04	0.09	0.06	0.07
2-MC_7	13.6	9.7	4.1	17.5	20.4	21.1	1.5	8.2	11.2
3-MC_7	13.7	9.2	5.5	17.9	25.4	23.2	2.3	11.9	12.6
4-MC_7	5.0	3.6	2.2	8.9	10.3	10.8	0.9	4.7	5.9
3-EC_6	1.7	1.3	0.8	4.8	4.8	5.9	0.5	2.5	3.1
2,2-DMC_6	0.8	0.2	0.5	0.8	1.5	2.9	0.3	0.8	0.8
2,3-DMC_6	1.5	0.6	0.3	1.4	2.1	3.1	0.4	1.4	1.5
2,4-DMC_6	2.7	1.1	1.4	2.7	4.2	5.9	0.7	2.5	2.7
2,5-DMC_6	2.4	0.9	0.9	2.2	2.6	3.7	0.5	1.6	1.9
3,3-DMC_6	0.4	0.1	0.3	0.3	1.0	2.1	0.1	0.5	0.5
3,4-DMC_6	0.8	0.4	0.4	1.1	1.9	2.4	0.3	1.1	1.5
3-E,2-MC_5	0.2	0.06	0.1	0.3	0.3	0.5	0.1	0.3	0.3
TMC_5	0	0	trace	Trace	Trace	Trace	0.04	Trace	0
Others	0.01	0.02	0.01	0.01	0	0	0.2	0	0
Conversion (%)	50.5	55.2	52.3	47.6	52.0	55.7	51.4	50.5	49.7

[a] Catalyst weight, 50 mg; varying *n*-octane feed rate with the same $H_2/n\text{-}C_8 = 16$; total pressure, 100 psig; temperature, 290°C; 1 h on stream.

[b] C_1–C_7 stand for alkanes from methane to heptanes; MC_5, methylpentanes; DMC_4, dimethylbutanes; DMC_5, dimethylpentanes; MC_6, methylhexanes; MC_7, methylheptanes; 3-EC_6, 3-ethylhexane; DMC_6, dimethylhexanes; 3-E,2-MC_5, methylethylpentane; TMC_5, trimethylpentanes; others, mainly alkylcycloalkanes.

The transformation of *n*-octane via various isomerization and cracking steps can be shown in Scheme 1.

The rates of the various isomerization and cracking steps were originally studied by Brower (28) for superacid homogeneous catalysts (HF) at relatively low temperature. Further study was carried out for metal-loaded zeolites and a refined reaction rate relation was proposed as follows (29, 30):

> hydride shift > type A cracking > type A isomerization (alkyl shift) > type B isomerization (PCP branching) > type B1 and B2 cracking > type C cracking > type D cracking.

Type B isomerization (PCP mechanism), which proceeds via protonated cyclopropane intermediates, predicts the following relative ratio among the three methylheptane isomers: 2-MC_7/3-MC_7/4-MC_7 = 1/2/1 from *n*-octane hydroisomerization (3). This product distribution is expected to occur only if the PCP mechanism is taking place. From the product distribution of methylheptanes we observed deviation from the predicted one based on the PCP mechanism (Table 6). This is because the products of the B-type isomerization of *n*-octane (monobranched C_8 isomers) are further transformed via type A isomerization reactions and finally approach the thermodynamic equilibrium (Table 6). Equilibrium compositions at 290°C in Table 6 are interpolated values based on calculation from thermodynamic data reported in the literature (31). It is worth noting that the above observation is valid in a wide range of Si/Al ratios (compare Beta-15 with Beta-132). The zeolite structure can impose steric constraints even on monobranched isomers. ZSM-12, possessing channels of smaller diameter in comparison with β-zeolite and USY, imposes transition state-type shape selectivity, thus favoring the formation of the less bulky 2-methyl and 3-methyl isomers. In addition, smaller amounts of 4-MC_7 and 3-EC_6 (3-ethylhexane) are observed over ZSM-12 than over USY and β-zeolites (Table 6).

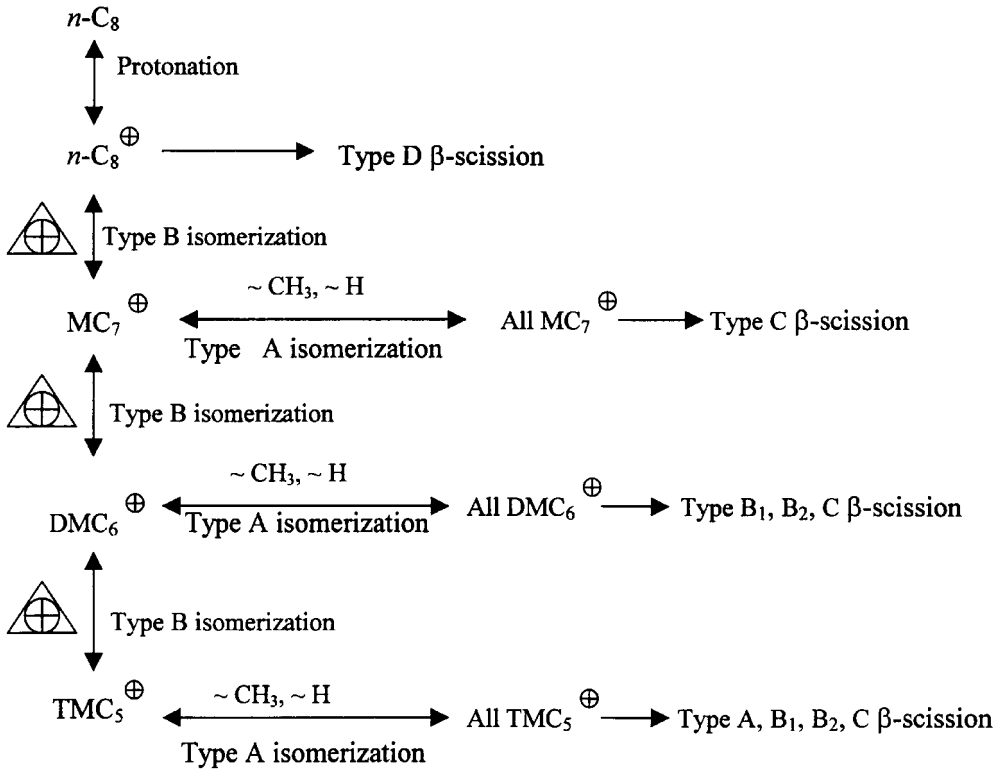

SCHEME 1. General isomerization and hydrocracking schemes of *n*-octane.

Regarding the dibranched octane isomer distributions, isomers with two branched alkyl groups on the same carbon of the main chain, i.e., 2,2-DMC_6 (2,2-dimethylhexane) and 3,3-DMC_6, are not favored in zeolites with relatively small openings. Indeed, we observed that the selectivities of the above dimethylhexanes are significantly lower than the values predicted by the thermodynamic equilibrium (Table 7). It should be noted that for zeolites with relatively large pores such as β-zeolite and USY the concentrations of the above isomers approach the equilibrium values. The selectivity of 2,3-DMC_6 is significantly higher than the equilibrium composition. The latter isomer is readily produced from several B-type isomerization reactions (PCP mechanism) of methylheptanes (Scheme 2, reactions 2.2 and 2.9). Due to the bulkier transition state intermediates of 2,2-DMC_6 and 3,3-DMC_6 and the space constraint imposed by the zeolite structure, their formation is not favored (see rows 1 and 5 in Table 7). Hence, 4-MC_7 is preferably transformed to the less bulky 2,3-DMC_6 via B-type isomerization (reaction 2.9); and 3-MC_7 is preferentially transformed to 3,4-DMC_6 and 2,4-DMC_6 (reactions 2.6 and 2.7 in Scheme 2). Our product distribution agrees very well with earlier findings (32). The present data indicate that the transformation of 2,3-DMC_6 to other dimethylhexanes is relatively slow. One should note that 2,4-DMC_6 can be generated by reactions 2.3 and 2.7 of Scheme 2, from 2-methylheptane and 3-methylheptane, while 2,5-DMC_6 is produced only by reaction 2.4 from 2-methylheptane. 2,4-DMC_6 follows the equilibrium compositions closely. All other dibranched isomers (2,5-DMC_6, 3,4-DMC_6, and 3-E,2-MC_5) are near equilibrium distribution. Another reason for the preferential formation of dibranched products

TABLE 6

Monobranched Product Isomer Distributions

Zeolite	ZSM-12-35	ZSM-12-69	Beta-15	Beta-132	USY-2.6	USY-28	MOR-9.5	MOR-36	LTL-3.8	Equilibrium
2-MC_7	39.9	40.9	32.6	35.6	33.5	34.6	28.6	29.9	34.2	32.5
3-MC_7	40.3	38.6	43.7	36.5	41.3	38.1	44.6	43.7	38.3	37.6
4-MC_7	14.7	15.2	17.5	18.1	17.1	17.6	17.8	17.2	18.1	12.5
3-EC_6	5.1	5.4	6.2	9.8	8.3	9.7	8.9	9.2	9.4	17.4

Note. *n*-Octane conversion: about 50% at 290°C (see Table 5).

TABLE 7

Dibranched Product Isomer Distributions

Zeolite	ZSM-12-35	ZSM-12-69	Beta-15	Beta-132	USY-2.6	USY-28	MOR-9.5	MOR-36	LTL-3.8	Equilibrium
2,2-DMC_6	9.6	6.8	12.1	8.7	11.1	14.2	12.8	9.6	9.5	15.2
2,3-DMC_6	17.2	17.3	17.9	16.5	15.7	14.8	15.7	17.3	17.1	7.1
2,4-DMC_6	30.4	31.3	31.0	31.4	30.5	28.6	30.8	30.8	30.5	27.6
2,5-DMC_6	26.9	26.8	19.5	24.9	19.2	18.0	19.8	19.8	21.2	24.8
3,3-DMC_6	4.9	3.9	6.4	3.1	7.5	10.4	5.3	5.7	5.7	12.9
3,4-DMC_6	9.1	11.3	9.9	12.1	13.9	11.7	11.8	13.4	12.2	9.7
3-E,2-MC_5	2.0	2.7	3.1	3.3	2.5	2.4	3.9	3.5	3.8	2.7

Note. n-Octane conversion: about 50% at 290°C (see Table 5).

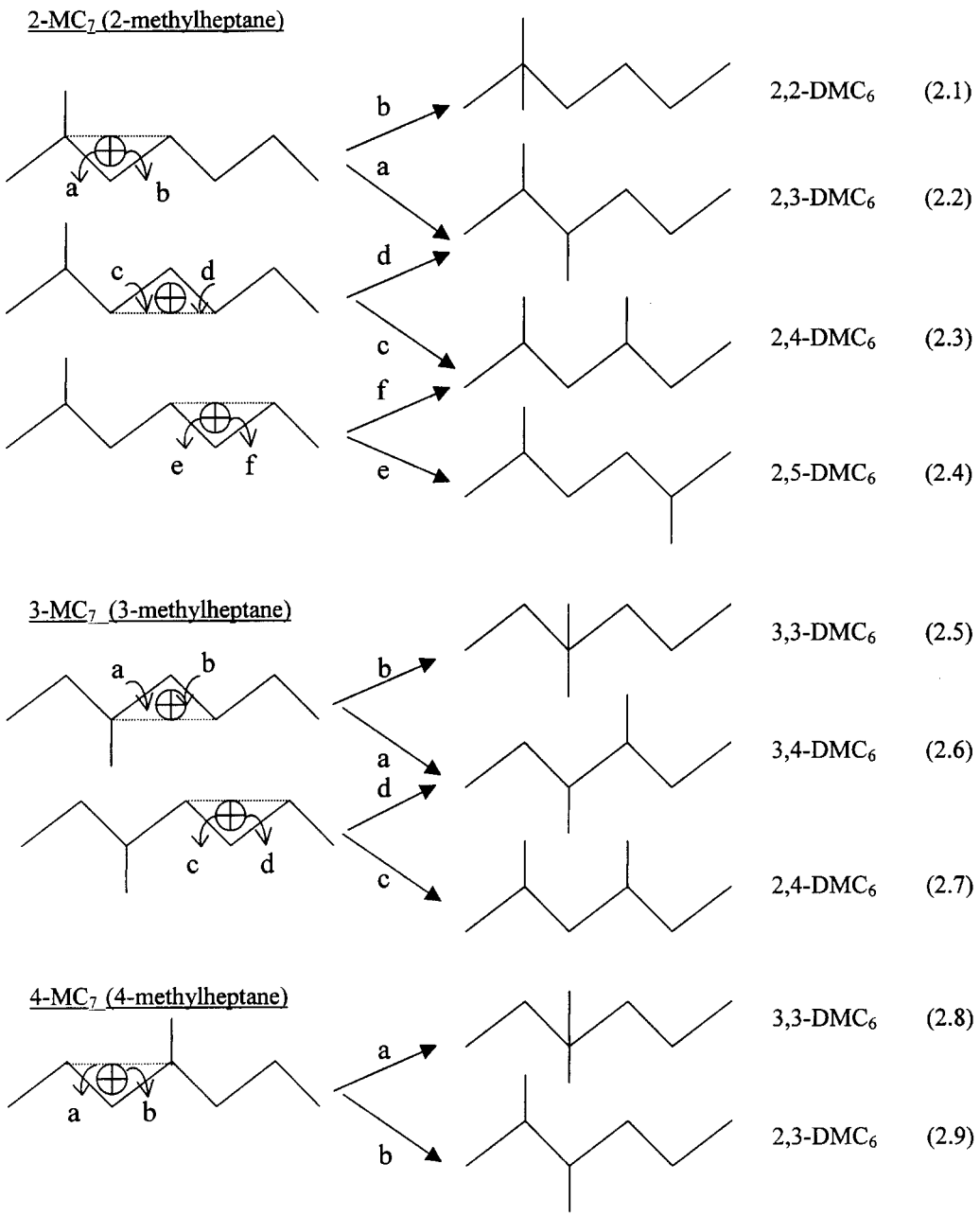

SCHEME 2. Formation of dimethylhexanes from monometylheptanes by protonated cyclopropane carbenium ions.

at the 2-position is the relatively faster type B isomerization of 2-MC_7 in comparison with other methylheptanes. It is reported that for methylheptanes, the rate of type B isomerization decreases in the order 2-MC_7 > 3-MC_7 > 4-MC_7 (33). This also explains why 2,2-DMC_6 is more abundant than 3,3-DMC_6. In other words, we observed a higher relative deviation from the equilibrium concentration for 3,3-DMC_6 than for 2,2-DMC_6. For the dibranched isomers containing ethyl branching, only 3-E,2-MC_5 is observed, and its concentration follows that predicted by equilibrium.

Lumped Product C_8 Isomer Selectivity versus Zeolite Acidity

C_8 isomer product selectivity is plotted versus *n*-octane conversion, and reveals the capability of each catalyst to favor the formation of branched isomers. The increase in the conversion is achieved by increasing the reaction temperature, while keeping the other operating conditions the same. Over β-zeolite catalysts the product C_8 isomer selectivities increase with the increase in Si/Al ratio (Fig. 3). Wang *et al*. (34) also observed a similar trend in a relatively narrow range of Si/Al ratios (from 18 to 30). An explanation for the increased product isomer selectivity is offered and it is based on the strength of the Brønsted acid sites.

The average Brønsted acid site strength of β-zeolite catalysts increases with the increase in the Si/Al ratio as verified by the NH_3-STPD experiments presented in Table 2. Since the isomerization proceeds through successive branching from normal to mono- to di-, and possibly to tribranched C_8 paraffins, high acid strength favors more branching. This is because high acid strength allows relatively longer residence time of the intermediate carbenium ions on the acid sites, thus providing sufficient time for the latter intermediates to be isomerized further. It should be noted that this is the case at relatively low temperatures where the cracking rate of the surface intermediates does not increase when the residence time on the acid site is relatively long. However, when the temperature increases above a certain level, the rate of the cracking increases. This can be seen in Fig. 3 where the isomerization selectivity drops significantly at high conversions (>70%) or equally high temperatures. Jacobs *et al*. (35) also found that high-acid-strength sites and a smaller number of weak sites reduce the rate of type A isomerization (via alkyl shift) and increase the rate of chain branching via protonated cyclopropane (PCP mechanism) intermediates at the same temperature. In this manner, more multibranched intermediates can be produced. It is also interesting to note that with the increase in the average acid site strength, the selectivity of cracked light paraffinic products decreases in the temperature range involved in this study. Chao *et al*. (36) also observed a similar decrease in cracking products with the increase in Si/Al ratio at the same level of conversion over Pt/HMOR and Pt/HBeta catalysts. Conclusively, under the mild reaction conditions involved in our study, hydroisomerization is favored at the expense of hydrocracking when Brønsted acid site strength is high.

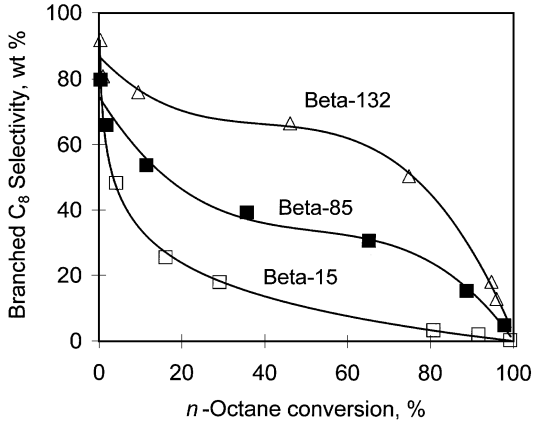

FIG. 3. Branched C_8 product selectivities versus conversion over Pt/HBeta at WHSV = 7 h^{-1}, H_2/*n*-C_8 (mole) = 16, total pressure of 100 psi, and Pt loading level of 0.5 wt%.

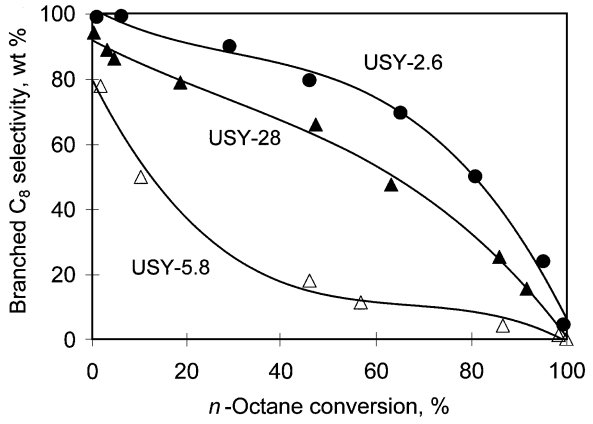

FIG. 4. Branched C_8 product selectivities versus conversion over Pt/HUSY at WHSV = 7 h^{-1}, H_2/*n*-C_8 (mole) = 16, total pressure of 100 psi, and Pt loading level of 0.5 wt%.

Similarly, over USY catalysts, we observe the same relation between C_8 isomer selectivity and Brønsted acid strength. More specifically, the C_8 isomer product selectivity does not change monotonically with Si/Al ratio (Fig. 4). One can observe that the selectivity for isomers decreases in the order USY-2.6 > USY-28 > USY-5.8 at any *n*-octane conversion. This trend indicates that the isomerization capability of USYs increases with the increase in the average Brønsted acid site strength. Our STPD experiments (Table 2) verified that the acid strength decreases in the same order: USY-2.6 > USY-28 > USY-5.8.

Over ZSM-12, the isomer product selectivities do not increase with the increase in Si/Al ratio (Fig. 5). Its acidity characteristics, presented in Table 2, indicate that the

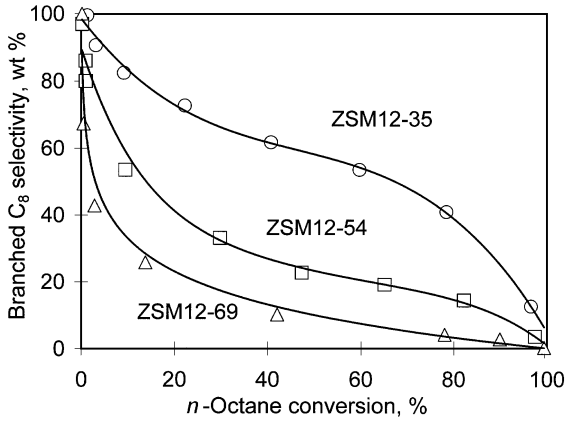

FIG. 5. Branched C_8 product selectivities versus conversion over Pt/HZSM-12 at WHSV = 7 h^{-1}, H_2/n-C_8 (mole) = 16, total pressure of 100 psi, and Pt loading level of 0.5 wt%.

average strong site strength slightly decreases with dealumination. These observations reinforce the general trend observed in our study with other zeolites that the hydroisomerization capability of a bifunctional catalyst increases with an increase in the average Brønsted strength.

A small number of experiments were also carried out at the same temperature (290°C) to verify that the selectivity differences discussed above are indeed due to the change in the acidic properties of the catalyst and not to the difference in temperature. The same trends as above are observed. More specifically, the increase in the Si/Al ratio of β-zeolite results in an increase in the selectivity of the branched octanes. On the other hand, for ZSM-12, as discussed earlier, the trend is reversed with the increase in Si/Al ratio. Thus, the effect of temperature on the total isooctane product selectivity is almost comparable to that of all zeolites with the same structure but different acidity. The different selectivity truly resulted from the difference in acidic site strength.

Distribution of Cracked Products

β-Scission of carbenium ions generated by the protonation of the parent and isomerized paraffins is the main reaction path for the fragmentation of alkanes over ideal bifunctional catalysts. The rate of cleavage of carbenium ions depends on the reaction temperature, acidity, and structure of the individual zeolite. No CH_4 was produced (Table 5), which indicates that hydrogenolysis does not occur over the catalysts tested under the reaction conditions discussed. The concentrations of hydrocarbons with six and seven carbon atoms were very low. This is as expected because the D type of β-scission (secondary to primary carbenium ions), which will produce C_1 and C_2 hydrocarbons by side cleavage of linear and branched carbenium ions, is energetically unfavorable. The majority of the cracked products possess three, four, and five carbon atoms. The fact that the concentrations of C_3 and C_5 hydrocarbons are almost equal (Table 5) indicates that they are the result of primary cracking of either linear or branched C_8 carbenium ions. An inspection of the C_5 product distribution indicates that zeolites with large pore openings such as USY favor the production of i-C_5. The very small concentration of C_2 hydrocarbon supports the fact that secondary cracking reactions do not take place except at very high reaction temperature. From the above discussion, one can conclude that the cracked products over all zeolites result from the primary hydrocracking of C_8 linear and branched carbenium ions.

Several possible β-scission routes exist for the further transformation of a branched intermediate carbenium ion. For instance, a 2-methylheptyl ion may crack according to the routes shown in Scheme 3. However, route 3.3 is the only feasible one since all the other routes involve a primary carbenium ion, which has a high activation energy barrier and is not favored (37). Based on this fact, the following analysis is limited to the most energetically favored reaction routes.

The most possible β-scission routes occurring for all normal and branched octyl carbenium ions on zeolites via type A, B_1, B_2, C, and D β-scissions are given in Scheme 4. Examining all the possible products of β-scission of C_8 carbenium ions with variable branching, one can conclude that only A and B types of β-scission are responsible for the direct production of i-butane. More specifically, type A β-scission (route 4.1) produces only i-C_4; type C and D scissions cannot produce any i-C_4. Routes 4.1 (from 2,2,4-TMC_5^+), 4.2 (from 2,2,3-TMC_5^+), 4.5 (from 2,2-DMC_6^+), and 4.6 (from 2,4-DMC_6^+) are responsible for the production of i-C_4 after the hydrogenation of the produced olefin. One should not forget that i-C_4 carbenium ions could finally desorb and result in i-butane. Routes 4.2 (from 2,2,3-TMC_5^+), 4.5 (from 2,2-DMC_6^+), 4.6 (from 2,4-DMC_6^+), 4.12 (from 3,4-DMC_6^+), 4.15 (from 3-MC_7^+), and 4.20 (from *n*-C_8^+) will lead to *n*-C_4. All other scission reactions produce neither i-C_4 nor *n*-C_4. The interconversion of isobutane and *n*-butane via the direct transformation of i-butane to *n*-butane through unimolecular isomerization of *tert*.-butyl carbenium ion followed by chain hydride transfer is minimal (38). This reaction could occur only at very high temperatures or concentrations. This is because it involves the formation of primary carbenium ions, which are energetically unstable. Another route for the interconversion of isobutane to *n*-butane goes through a bimolecular mechanism, which requires very strong Brønsted acid sites, long contact time, and relatively high temperature (39). The presence of hydrogen (hydrogenation of intermediate olefins) further inhibits the above bimolecular pathway, since the C_4 carbenium ions required for the alkylation step are in very low concentration (40). Indeed, from our experiments we found that the hydroconversion of isobutane over the zeolite catalysts used in the current study is negligible, unless the reaction temperature

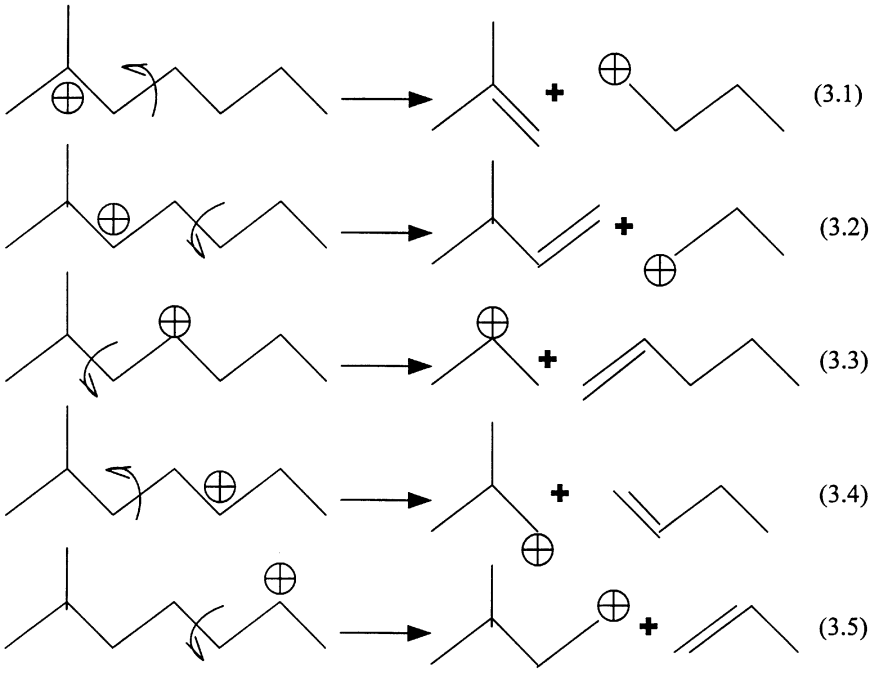

SCHEME 3. Possible β-scission routes of 2-methylheptyl ion.

is above 350°C (Table 8). Considering the coexistence of other high-molecular-weight paraffins, the reaction of i-butane is even lower. Other researchers (41) found that the longer alkanes in mixtures are preferentially converted due to competitive adsorption favoring the heavy compounds. Therefore, one can conclude that the produced normal and isobutanes result from the primary β-scission modes, unless either the conversion or temperature is high.

With the increase in reaction temperature, the i-C_4/n-C_4 ratio significantly decreases for high-Al-content zeolites (USY and nondealuminated β-zeolite), and it does not change that much for low-Al-content zeolite catalysts such as Beta-132 (Fig. 6). Other researchers also found that with the increase in Si/Al ratio, the i-C_4/n-C_4 ratio decreases for *n*-hexane isomerization over mordenite (42), and for

TABLE 8

Product Yields of i-C_4 Hydroconversion over Zeolite Catalysts[a]

Catalyst	Temperature (°C)	Conversion (%)	Isomerization yield (%)[b]	Disproportionation yield (%)[c]
ZSM-12-35	290	0.9	0.5	0.4
	350	4.2	1.3	2.9
	400	13.9	6.8	5.3
Beta-15	290	0.2	0.2	0.0
	350	3.7	3.3	0.3
	400	12.8	9.7	1.5
	450	33.7	24.7	6.4
USY-2.6	290	0.2	0.1	0.1
	350	1.0	0.3	0.2
	400	7.7	4.0	0.8
	450	22.4	14.9	2.4
MOR-9.5	290	0.9	0.6	0.3
	350	18.7	12.3	6.4
	400	49.1	21.2	27.3

[a] Reaction conditions: H_2/i-C_4 (mole) = 6, WHSV = 10 h^{-1}, Pt loading level of 0.5 wt% on all catalysts, 10 min on stream.
[b] n-C_4 paraffin and olefin.
[c] C_3, C_5 paraffins and olefins.

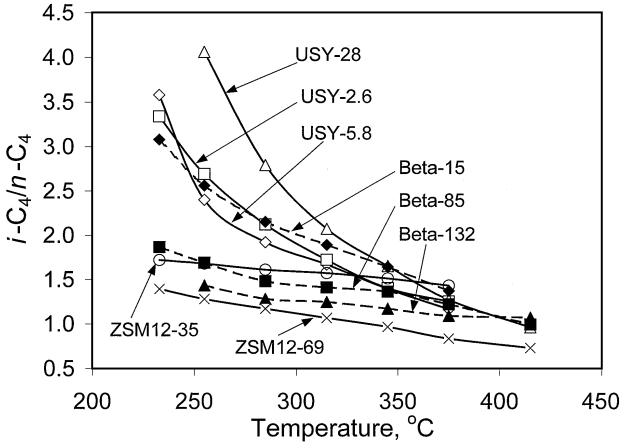

FIG. 6. i-C_4/n-C_4 ratio of cracked products from *n*-octane hydroconversion versus temperature at WHSV = 7 h^{-1}, H_2/n-C_8 (mole) = 16, total pressure of 100 psi, and Pt loading level of 0.5 wt%.

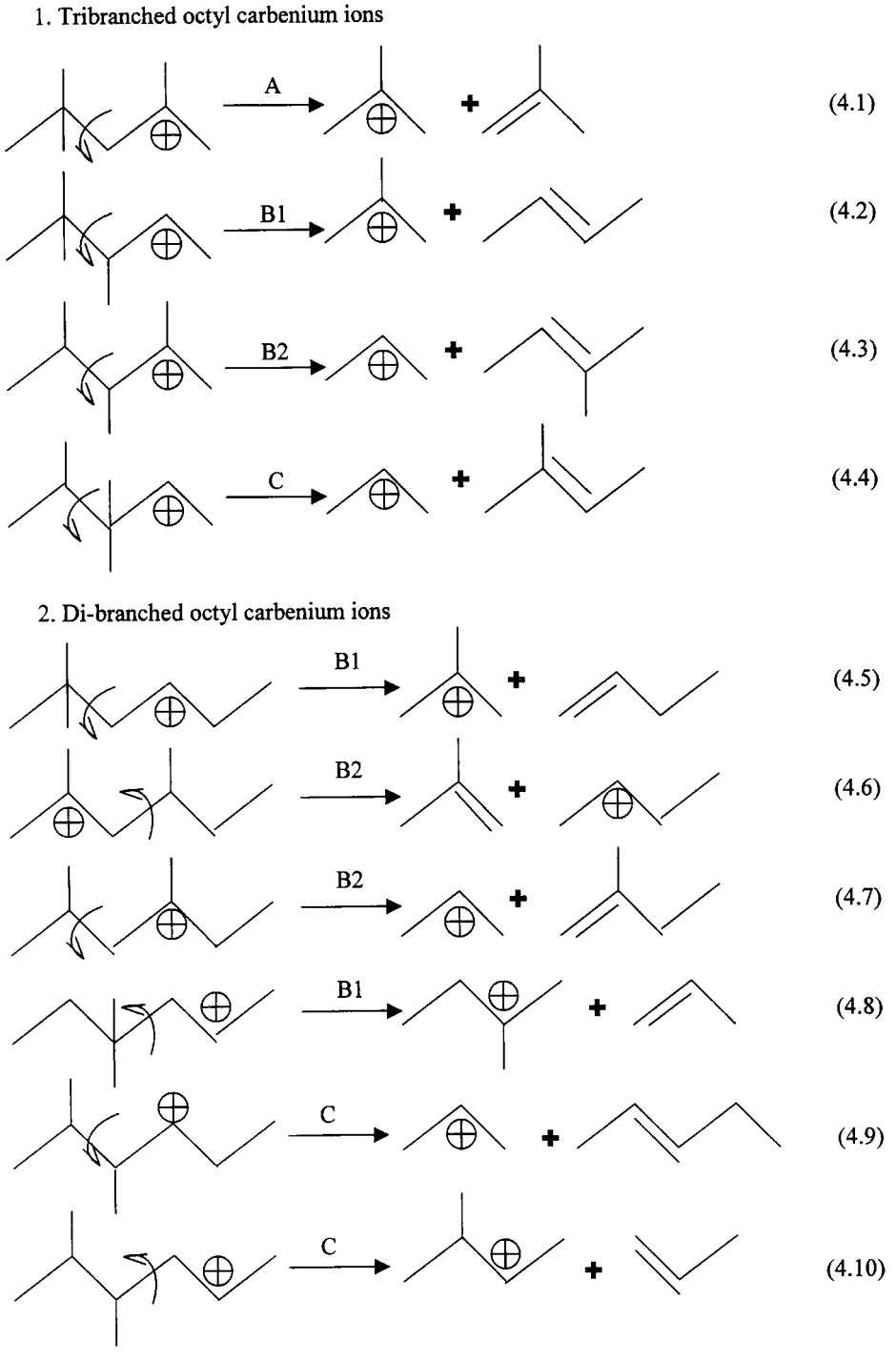

SCHEME 4. Energetically favored β-scission modes of various octyl carbenium ions.

decane hydroisomerization–hydrocracking reaction over some USY zeolites (43). By looking at all the possible β-scissions of C_8 carbenium intermediates (reactions 4.1 to 4.21), one can observe that i-C_4 can be produced as a primary product only by A and B types of scission. More specifically, type A scission (reaction 4.1) is responsible for generating potentially two i-butane molecules. Type B scission is also responsible for the production of i-butane. According to the relative order of rates for isomerization and cracking presented earlier in this paper, type A scission is significantly faster than B, C, and D types of cracking. The latter two types of scission can generate only normal butane.

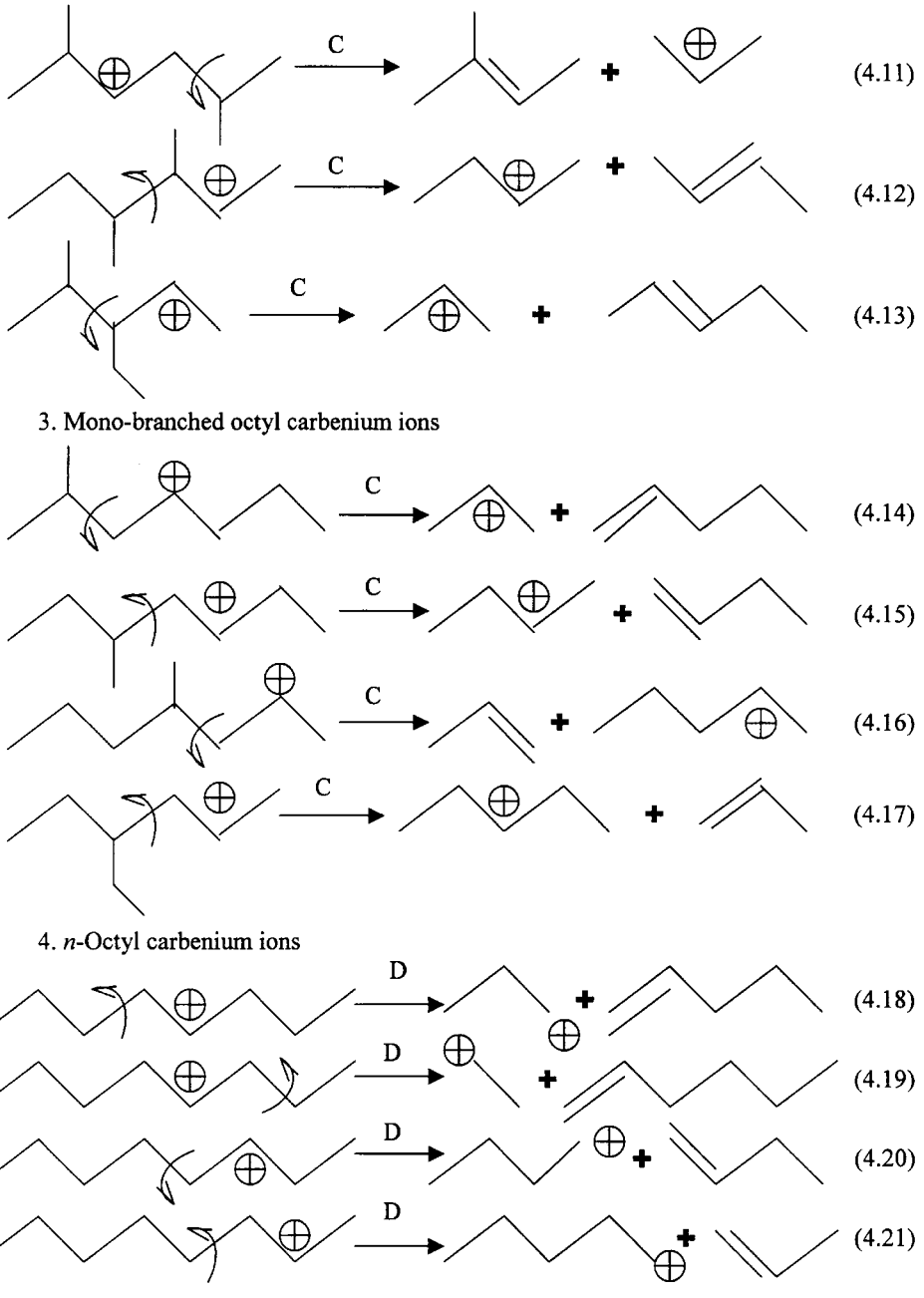

SCHEME 4—*Continued*

From our experiments, it seems that for high-Al-content zeolites (USY-2.6, -5.8, -28, and Beta-15), type A cracking (reaction 4.1) dominates over the other scission mechanisms. The transformation of 2,2,4-trimethylpentane ion via reaction 4.1 will shift the equilibrium among all the trimethylpentane carbenium ions toward the former isomer (2,2,4-TMC_5^+). On the other hand, 2,2,4-trimethylpentane is the most abundant tribranched isomer thermodynamically (Fig. 7). In this way, the i-C_4/*n*-C_4 ratio acquires high values. By increasing the temperature, the equilibrium concentration of 2,2,4-trimethylpentane decreases significantly, and thus the contribution of type A scission (reaction 4.1), which produces isobutane, diminishes. Moreover, the difference between the reaction rates of types A, B, C, and D decrease with increasing temperature (3, 27, 44), thus resulting in the decrease in the relative production of i-C_4. It should also be noted that with the increase in temperature, the equilibrium concentrations of 3-MC_7 and 3,4-DMC_6 increase significantly (Fig. 7). This means that relatively more *n*-butane can be produced via reactions 4.12 and 4.15, respectively.

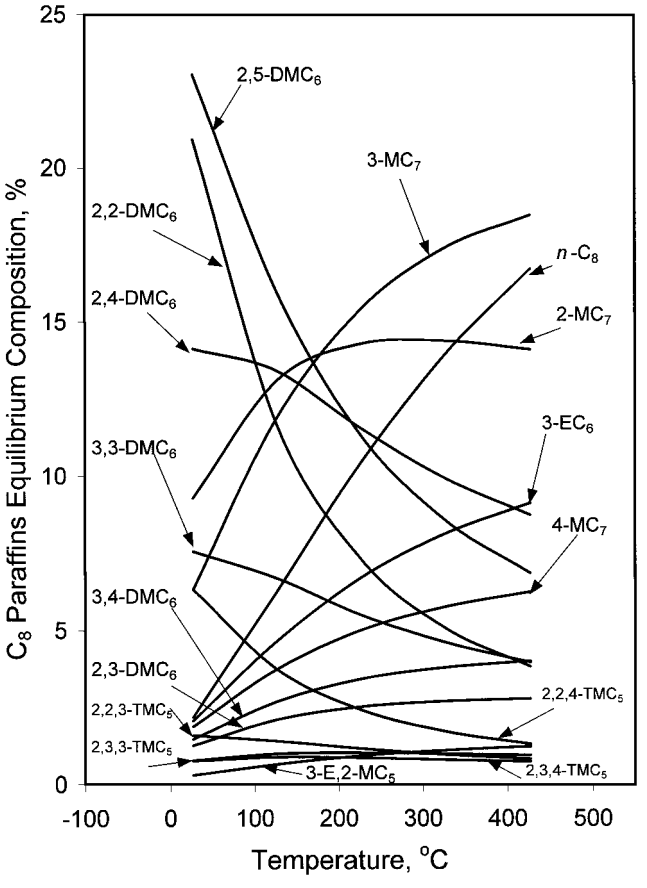

FIG. 7. Thermodynamic equilibrium of normal, monobranched, dibranched, and tribranched octanes versus temperatures.

On the other hand, for zeolite catalysts with relatively low aluminum content (ZSM12-35, -69, Beta-85, -132), we observe that the i-C_4/*n*-C_4 ratio at low temperature decreases significantly in comparison with the Al-rich zeolites. The increase in temperature does not alter significantly the above ratio. This is evidence that the role of type A scission (reaction 4.1) diminishes while B_1, B_2, and C types of scission become dominant.

Time-on-Stream Behavior

Accelerated coking experiments were carried out to test the resistance of the zeolites to deactivation. Significantly higher WHSV and lower H_2/*n*-octane ratios than in the usual experiment were used to expedite the deactivation of the catalysts in the accelerated coking experiments. USY-2.6 lost almost 50% of its initial activity in about 60 h on stream due to the deactivation resulting from carbonaceous deposit (Fig. 8). The selectivities of isomers and light cracked products also change significantly with time. More specifically, the isomerization capability of USY increases while that of cracking decreases. This is because during the initial stages of the reaction, the strongest acid sites, which are responsible for hydrocracking, are deactivated. USY has supercages of 12.2 Å connected with channels of 7.4 Å, favoring the accumulation of coking precursors, which result in fast deactivation of the above catalyst.

It is remarkable to note that ZSM-12 does not lose any of its initial activity over 1100 h on stream under the same severe conditions. The product selectivities and yields are also very stable as a function of time. In our previous investigation (4, 45), we observed this superior performance of ZSM-12 for the reforming of naphthenic mixtures at higher temperatures (vicinity of 470°C). The superior stability of ZSM-12 even under accelerating coking conditions results from its unique pore structure, which does not favor coke formation. Its unidimensional noninterpenetrating puckered channels (5.6×6.1 Å) act as perfect tubes, which do not trap coke precursors (Fig. 9). This unique pore structure renders ZSM-12 an excellent zeolite to withstand coke deactivation. We also found that L-zeolite, although it also possesses a one-dimensional configuration of pores (7.1 Å), deactivates fast. This is because of the existence of periodic expansions along the channels with dimensions of about 13 Å (46). Coke precursors probably tend to accumulate in these expansions of the pores.

CONCLUSION

Both the zeolite acidity (number and strength distribution) and the pore structure play very important roles in the conversion and product selectivity for the hydroconversion of *n*-paraffins. Catalytic activity per acidic site (TOF) at the initial stages of the reaction (1 h on stream) and for comparable Si/Al ratios decreases in the following order: ZSM-12 > β-zeolite > mordenite > USY > L-zeolite.

ZSM-12 demonstrated superior stability in the accelerated coking experiments. The superior behavior of ZSM-12

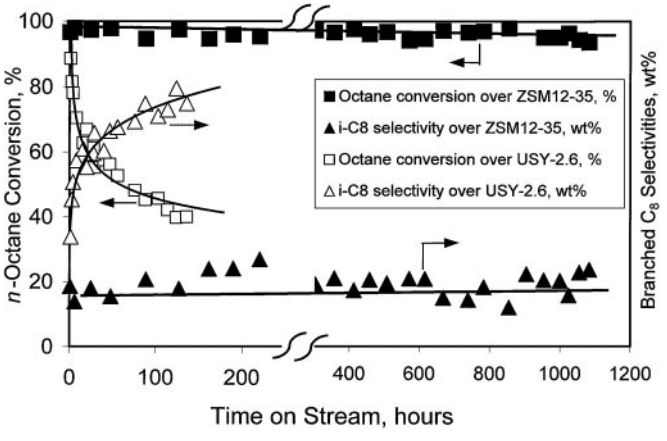

FIG. 8. Time-on-stream behavior of *n*-octane hydroconversion over ZSM-12 (290°C) and USY (320°C) zeolites at the accelerating deactivation conditions (WHSV = 11.2 h^{-1}, H_2/*n*-C_8 = 4, total pressure of 100 psig, and Pt loading level of 0.5 wt%).

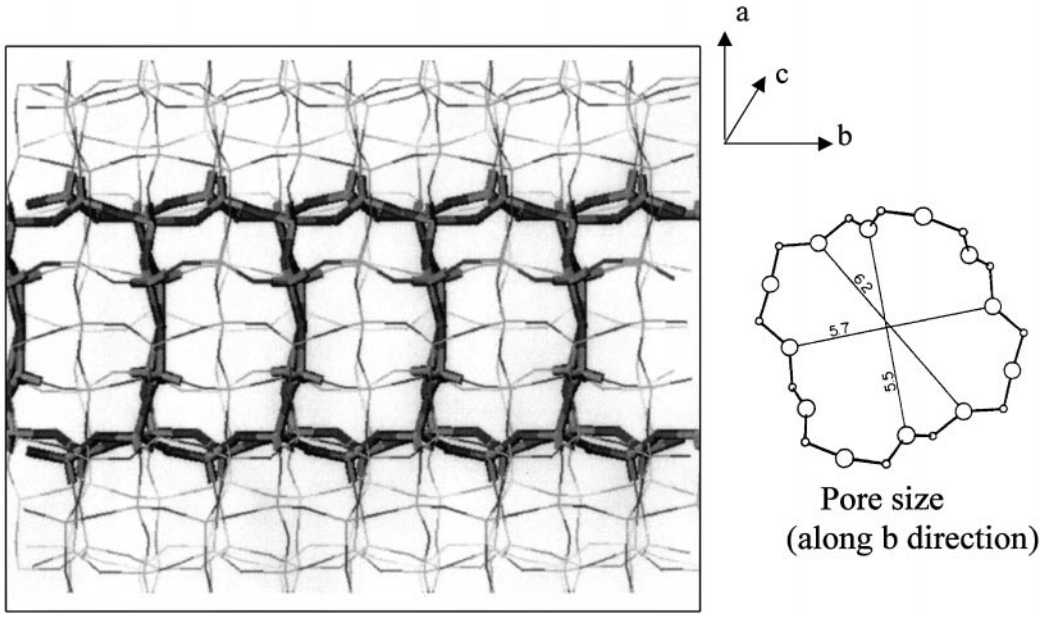

FIG. 9. Schematic of the ZSM-12 pore structure.

even under accelerated coking conditions results from its unique pore structure, which does not favor coke formation. Its one-dimensional noninterpenetrating puckered channels (5.5×6.1 Å) act as perfect tubes, which do not trap coke precursors.

Branched product selectivity increases with an increase in Brønsted acid site strength of the zeolite catalysts, and thus hydroisomerization is favored at the expense of cracking at a higher Brønsted acid strength in the temperature range studied. 2,2-DMC_6 and 3,3-DMC_6 are not favored in final products due to their bulky molecular size even in USY. In addition, the 2,2-DMC_6 species is more abundant than 3,3-DMC_6 because the rate of isomerization by PCP intermediates decreases in the following order: 2-MC_7 > 3-MC_7 > 4-MC_7. The concentration of 2,3-DMC_6 is much higher than equilibrium, which indicates that the interconversion of 2,3-DMC_6 to other dibranched isomers is not preferred. The i-C_4/*n*-C_4 ratio detected depends on both the reaction temperature and zeolite pore structure/acidity. The aluminum content determines the type of β-scission reactions. For zeolites with high concentration of acid sites (Si/Al < about 30), type A β-scission dominates at low temperature, while at lower Al content type A, B, and C β-scissions are equally important.

USY-5.8 (CBV-712) showed relatively high activity with respect to other USYs. This is probably related to its high surface Al content. The Brønsted acid strength of the USY zeolites decreases in the order USY-2.6 > USY-28 > USY-5.8. There is a linear relation between Brønsted site strength and branched isomer selectivity during hydroisomerization of *n*-octane.

ACKNOWLEDGMENTS

The authors acknowledge financial support from the National Science Foundation through a CAREER award (CTS-9702081). Acknowledgment is also made to the donors of the Petroleum Research Fund (ACS) for the support of this research through Grant ACS-PRF 316065-G5.

REFERENCES

1. Giannetto, G., Perot, G., and Guisnet, M., *Ind. Eng. Chem. Prod. Res. Dev.* **25**, 481 (1986).
2. Martens, J. A., Tielen, M., and Jacobs, P. A., *Stud. Surf. Sci. Catal.* **46**, 49 (1989).
3. Martens, J. A., and Jacobs, P. A., *in* "Theoretical Aspects of Heterogeneous Catalysis" (J. B. Moffat, Ed.), p. 52. Van Nostrand Reinhold, New York, 1990.
4. Smirniotis, P. G., and Zhang, W., *Ind. Eng. Chem. Res.* **35**, 3055 (1996).
5. Robb, G., Zhang, W., and Smirniotis, P. G., *Microporous Mesoporous Mater.* **20**, 307 (1998).
6. Zhang, W., Burckle, E., and Smirniotis, P. G., submitted for publication.
7. Maache, M., Janin, A., Lavalley, J. C., and Benazzi, J. E., *Zeolites* **13**, 419 (1993).
8. Chen, D., Sharma, S., Cardona-Martinez, N., Dumesic, J. A., Bell, V. A., Hodge, G. D., and Madon, R. J., *J. Catal.* **136**, 392 (1992).
9. Haag, W. O., and Lago, R. M., U.S. Patent 4,326,994 (1982).
10. Datka, J., Marcchmeyer, S., Neubauer, T., Meusinger, J., Papp, H., Schutze, F.-W., and Szpyt, I., *J. Phys. Chem.* **100**, 14451 (1996).
11. Graham, J. H., Burrows, C., Rhodes, C., Kiely, C. J., and McClung, R., *J. Chem. Soc. Faraday Trans.* **93**, 3593 (1997).
12. Farneth, W. E., and Gorte, R. J., *Chem. Rev.* **95**, 615 (1995).
13. Kuehne, M. A., Babitz, S. M., Kung, H. H., and Miller, J. T., *Appl. Catal. A* **166**, 293 (1998).
14. Remy, M. J., Stanica, P., Poncelet, G., Feijen, E. J. P., Grober, P. J., Martens, J. A., and Jacobs, P. A., *J. Phys. Chem.* **100**, 12440 (1996).
15. Derouane, E. G., Andre, J., and Lucas, A. A., *J. Catal.* **110**, 58 (1988).

16. Wojciechowski, B. W., and Corma, A., *in* "Catalytic Cracking Catalysts, Chemistry, and Kinetics." Marcel Dekker, New York, 1986.
17. Dai, P. E., Neff, L. D., and Ewards, J. T., *in* "Fluid Catalytic Cracking III" (M. L. Occeli and P. O'Connor, Eds.), p. 63. Am. Chem. Soc., Washington, DC, 1994.
18. Dadyburjor, D. B., and Bellare, A., *J. Catal.* **126**, 261 (1990).
19. Boulet, M., Bourgeat-Lami, E., Fajula, F., Des Courieres, T., and Garrone, E., *in* "Proceedings, 9th International Zeolite Conference, Montreal, 1992," Vol. 2, p. 389.
20. Benslama, R., Fraissard, J., Albizane, F., Fajula, F., and Figueras, F., *Zeolites* **8**, 196 (1988).
21. LaPierre, R. B., Rohrman, A. C., Schlenker, J. L., Wood, J. D., Rubin, M. K., and Rohrbaugh, W. J., *Zeolites* **5**, 346 (1985).
22. Choudhary, V. R., and Akolekar, D. B., *J. Catal.* **117**, 542 (1989).
23. Meriaudeau, P., Tuan, V. A., Nghiem, V. T., Lai, S. Y., Hung, L. N., and Naccache, C., *J. Catal.* **169**, 55 (1997).
24. Zhang, W., and Smirniotis, P. G., Hydrocracking and hydroisomerization of branched octanes over large pore zeolites, in preparation, 1998.
25. Fyfe, C. A., Gies, H., Kokotailo, H., Marler, B., and Cox, D. E., *J. Phys. Chem*. **94**, 3718 (1990).
26. Csicsery, S. M., *J. Catal.* **23**, 124 (1971).
27. Martens, J. A., Jacobs, P. A., and Weitkamp, J., *Appl. Catal. A* **20**, 239 (1986).
28. Brouwer, D. M., *in* "Chemistry and Chemical Engineering of Catalytic Processes" (R. Prins and G. C. A Schuit. Eds.), NATO ASI Seres E, No. 39, p. 137. Sijthoff & Noordhoff, 1980.
29. Weitkamp, J., and Farag, H., *Acta Phys. Chem*. **2**, 327 (1978).
30. Jacobs, P. A., Martens, J. A., Weitkamp, J., and Beyer, H. K., *Faraday Disc. Chem. Soc.* **72**, 353 (1982).
31. Stull, R. D., Westrum, E. F., and Sinke, G. C., "The Thermodynamics of Organic Compounds." Wiley, New York, 1969.
32. Weitkamp, J., *in* "Hydrocracking and Hydrotreationg, ACS Symp. Ser., Vol. 20, p. 1. Am. Chem. Soc., Washington, DC, 1975.
33. Weitkamp, J., *Ind. Eng. Chem. Prod. Res. Dev.* **21**, 550 (1982).
34. Wang, Z. B., Kamo, A., Yoneda, T., Komatsu, T., and Yashima, T., *Appl. Catal. A* **159**, 119 (1997).
35. Jacobs, P. A., Martens, J. A., and Beyer, H. K., *in* "Catalysis by Acids and Bases" (B. Imelik, C. Naccache, G. Coudurier, Y. Ben Taarit, and J. C. Vedrine, Eds.), Stud. Surf. Sci. Catal., Vol. 20, p. 399 (1985).
36. Chao, K.-J., Wu, H.-C., and Leu, L.-J., *Appl. Catal. A* **143**, 223 (1996).
37. Vogel, P., "Carbocation Chemistry." Elsevier, Amsterdam, 1985.
38. Stocker, M., Hemmersbach, P., Roeder, J. H., and Grepstad, J. K., *Appl. Catal. A* **25**, 223 (1986).
39. Guisnet, M., and Gnep, N. S., *Appl. Catal. A* **146**, 33 (1996).
40. Tran, M.-T., Gnep, N. S., Guisnet, M., and Nascimento, P., *Catal. Lett.* **47**, 57 (1997).
41. Denayer, J. F., Baron, G. V., Souverijns, W., Martens, J. A., and Jacobs, P. A., *Ind. Eng. Chem. Res.* **36**, 3242 (1997).
42. Guisnet, M., *Appl. Catal. A* **71**, 283 (1991).
43. Corma, A., Martinez, A., Pergher, S., Peratello, S., Perego, C., and Bellusi, G., *Appl. Catal. A* **152**, 107 (1997).
44. Martens, J. A., Tielen, M., and Jacobs, P. A., *Catal. Today* **1**, 435 (1987).
45. Zhang, W., and Smirniotis, P. G., *Appl. Catal. A* **168**, 113 (1998).
46. Newsam, J. M., *J. Phys. Chem*. **93**, 7689 (1989).